Geological Society of America
Special Paper 307
1996

Geochemistry of the Frasnian-Famennian boundary in Belgium: Mass extinction, anoxic oceans and microtektite layer, but not much iridium?

P. Claeys*
Department of Geology and Geophysics, University of California, Berkeley, California 94720-4767
F. T. Kyte
Institute of Geophysics and Planetary Physics, University of California, Los Angeles, California 90024
A. Herbosch*
Department of Geology and Geophysics, University of California, Berkeley, California 94720-4767
J.-G. Casier
Paleontology Department, Belgian Royal Institute of Natural Sciences, 29 Rue Vautier, B-1040 Brussels, Belgium

ABSTRACT

The Late Devonian, and in particular the Frasnian-Famennian (F/F) boundary, records one of the five largest mass extinctions in the fossil record. Glassy spherules believed to be of impact origin are associated with the F/F boundary in two Belgian sections (Senzeille and Hony). They have also been reported in sediments deposited approximately 1.5 to 2 m.y. above the boundary in south China, and in the Canning Basin (Australia) this event coincides with a 300 pg/g Ir anomaly. In this study, the F/F boundary in the Hony section was analyzed for trace and major elements to test the possibility of an Ir anomaly associated with the spherule layer. No significant positive Ir anomaly was detected in the 2 m of section investigated. Nevertheless, chalcophile elements show an increase within the dark shale bed marking the F/F boundary. This increase is interpreted to represent a reduction in oxygen concentrations in the depositional environment. This level must be equivalent to the upper part of the Kellwasser anoxic event recognized throughout the paleo-Tethys in what is now western Europe. The F/F boundary seems to be marked by a succession of major events, including impact, oxygen-depleted water on the shelf, and worldwide extinction of organisms.

INTRODUCTION

The Cretaceous-Tertiary (K/T) boundary debate has triggered intense searches for evidence of possible impact-related mass extinctions in the fossil record. So far, only at the K/T boundary is there significant evidence to support an impact-extinction linkage. The Late Devonian, and more particularly the Frasnian-Famennian (F/F) boundary, corresponds to one of the five largest mass extinction periods in the fossil record (Sepkoski, 1982) and is characterized by the disappearance of pelagic and shallow benthic organisms and reef builders (McLaren, 1982). Possible impact products in the form of glassy microtektite-like spherules have been documented recently at or near the F/F boundary in Late Devonian sections in south China and Belgium (Wang, 1992; Claeys et al., 1992; Claeys and Casier, 1994). In China the glass spherules are found 1.5 to 2 m.y. above the F/F

*Present addresses: Claeys, Institut für Mineralogie, Museum für Naturkunde, Invalidenstrasse 43, D-10015 Berlin, Germany; Herbosch, Earth and Environmental Sciences Department, CP 160, Free University of Brussels, 50 Avenue F. D. Roosevelt, B-1050 Brussels, Belgium.

Claeys, P., Kyte, F. T., Herbosch, A., and Casier, J-G., 1996, Geochemistry of the Frasnian-Famennian boundary in Belgium: Mass extinction, anoxic oceans and microtektite layer, but not much iridium?, *in* Ryder, G., Fastovsky, D., and Gartner, S., eds., The Cretaceous-Tertiary Event and Other Catastrophes in Earth History: Boulder, Colorado, Geological Society of America Special Paper 307.

boundary and are stratigraphically equivalent to a small Ir anomaly detected in the Canning Basin in Australia (Playford et al., 1984; Nicoll and Playford, 1990; Wang, 1992). In the Hony section in Belgium, the glass spherules occur a few centimeters above where Sandberg et al. (1988) placed the boundary (Claeys and Casier, 1994). In the Senzeille section in Belgium, 95 km southwest of Hony, the spherule layer is found in basal Famennian strata (Claeys et al., 1992), but the exact stratigraphic position remains unclear because of the lack of reliable conodont biostratigraphy in this section.

Previous studies had failed to show an Ir anomaly associated with the F/F boundary in European and American Late Devonian sections (Orth et al., 1990). The F/F boundary in the Sinsin section in Belgium was unsuccessfully investigated for Ir (McGhee et al., 1984), but that section has a small (40- to 50-cm) gap in sedimentation precisely at the F/F boundary (Streel and Vanguestaine, 1989; Casier and Devleeschouwer, 1994). This gap seems to correspond to the fine dark shale bed containing the spherule layer in Hony. Only in the basal Famennian of the Canning Basin has a small (300 pg/g) Ir anomaly been found in what was then believed to be the Upper *triangularis* conodont Zone (Playford et al., 1984). The increase in Ir was attributed to Ir extraction and concentration from seawater by *Frutexites* algae and bacteria (Playford et al., 1984). Recently, Nicoll and Playford (1990) reevaluated the stratigraphic position of the Ir anomaly and moved it to the lower *crepida* Zone, which is precisely the same stratigraphic level as the Chinese glass spherules.

This chapter presents a multielement geochemical profile across the F/F boundary in the Hony section. The goal of this investigation was to search for a positive Ir anomaly or any other geochemical anomaly associated with the dark shales containing the microtektite-like layer just above the F/F boundary.

THE F/F BOUNDARY MASS EXTINCTION AND THE HONY SECTION

The Hony section is located in the northeastern part of the Dinant Basin in Belgium (Fig. 1). The section provides a continuous exposure of upper Frasnian to lower Famennian strata consisting of olive-green to gray shales, frequently interrupted by beds of coarse bioclastic limestone a few centimeters to a few decimeters thick (Fig. 2). Locally, carbonate nodules of diagenetic origin occur in the shale. The carbonate bioclastic beds are graded, exhibit sharp or erosional bases, and are mainly formed by fragments of brachiopods, crinoids, and, locally, ostracodes. These bioclastic beds are typical storm deposits or tempestites (Flügel, 1982). The depositional setting appears to have been the outer shelf—well under fair-weather wave base but within the zone frequently reworked by storms.

The F/F boundary was recently defined by the International Sub-Commission on Devonian Stratigraphy as the base of the Lower *triangularis* conodont Zone, and the type section was chosen at Coumiac in southern France. In Hony, the Lower *triangularis* conodont Zone is separated from the uppermost Frasnian *linguiformis* conodont Zone by approximately 150 cm of shale containing no identifiable conodont taxa (Sandberg et al., 1988). This interval has been studied and sampled in detail for the present study and is subdivided into two units (Fig. 2). At the base is 110 cm of massive gray shales containing thin (millimeter-scale) layers of storm-transported coquinoid accumulation. The intensity and frequency of the storm beds appears to decrease upward across the 110 cm. This is inferred from thickening of the massive shales, thinning of the interlayered coquina, and reduction in the size of the bioclasts. The upper unit consists of 40 cm of finer and more fissile dark-gray shales and probably represents a deepening of the depositional environment. In thin section these shales show well-preserved fine quartz silt laminae with some larger basal bioclasts, interpreted as characteristic of very distal tempestites. The shale lacks bioturbation, and its faunal content is low, except for a few ostracod valves. This unit is lithologically different from the overlying olive-green basal Famennian shales, which are more massive and contain abundant crinoids, brachiopods, and some ostracodes.

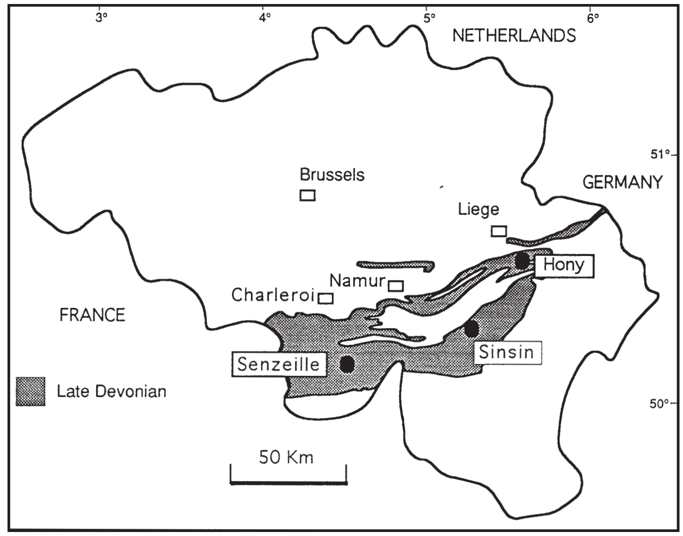

Figure 1. Map of Belgium showing Late Devonian strata and the location of the Hony (Long: E5°34′5″; Lat: N50°32′30″), Senzeille (Long: E4°27′30″; Lat: N50°09′42″), and Sinsin sections (Long: 5°14′00″; Lat: 50°16′40″).

Sandberg et al., (1988) placed the F/F boundary at the base of this 40 cm dark-gray shale (Fig. 2), based on stratigraphic correlation with the Steinbruch Schmidt F/F boundary section in Germany. At Steinbruch Schmidt, the uppermost Frasnian *linguiformis* conodont Zone is marked by anoxic black bituminous limestones and shales of the upper Kellwasser horizon. This Kellwasser horizon is also recognized in the type section at Coumiac in the form of dark dolomitic mudstones with a positive δC^{13} (≈3‰) anomaly indicating

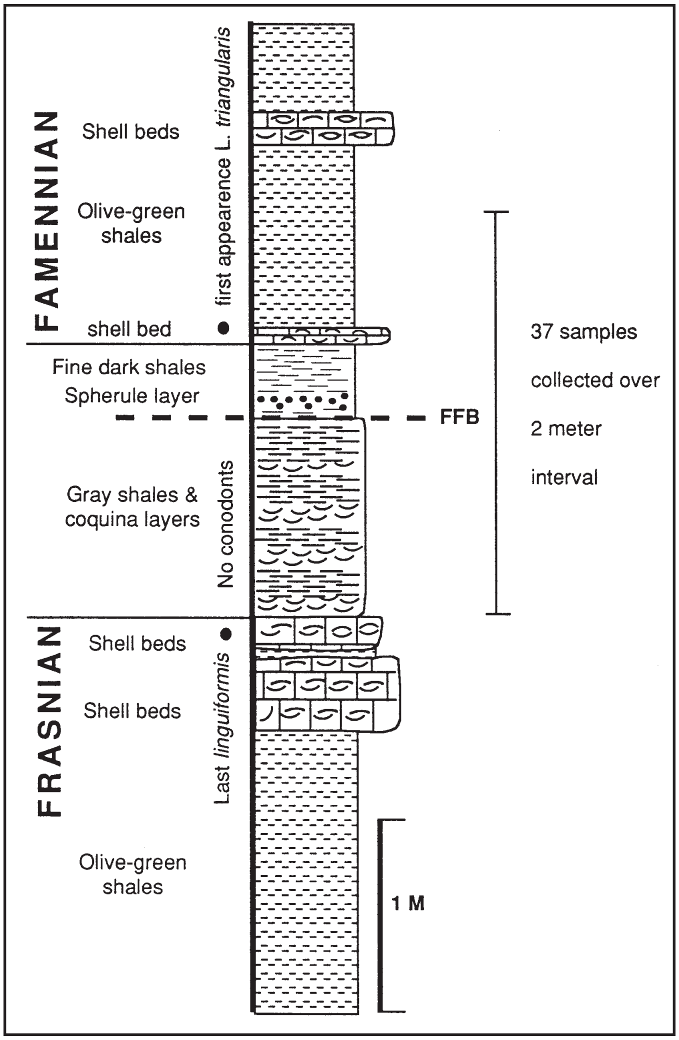

Figure 2. Stratigraphic and lithologic column of the Hony F/F boundary section showing the spherule layer, the changes in lithology, the conodont zonation, and the interval sampled for this study. Location of F/F boundary after Sandberg et al., 1988.

anoxic conditions (Joachimski and Buggisch, 1993). In Coumiac the F/F boundary is located directly above this anoxic horizon (Becker et al., 1989).

In the Hony section, the late Frasnian mass extinction occurred at the base of, or within, the 110-cm-thick bed of gray shales containing storm-generated coquinoid layers (Sandberg et al., 1988). Streel and Vanguestaine (1989) have demonstrated a strong decrease in the abundance of acritarchs, miospores, and other palynomorphs in the dark shale bed above the boundary. They attribute this reduction to a sudden increase in sedimentation rate. In Coumiac, extinction of organisms appears to begin 1 or 2 m below the boundary but seems to culminate in the upper Kellwasser horizon for goniatites, conodonts, and ostracodes and a few centimeters below this horizon for trilobites (Fig. 3 *in* Becker et al., 1989; Lethiers and Casier, 1995).

SAMPLING AND ANALYTICAL TECHNIQUES

This study of major and trace elements is probably one of the most extensive undertaken at the F/F boundary anywhere. The data presented in this study also contribute to the database on the composition of Paleozoic shales. The Hony section was selected for this study because (1) it contains glasslike microtektites just above the F/F boundary, (2) it is well constrained by conodont biostratigraphy, and (3) it probably represents continuous deposition across the F/F boundary.

The F/F boundary was sampled in great detail for this study; 37 samples were taken from a 2-m interval of shale beds above and below the boundary (Fig. 2). In the dark shale bed containing the spherule layer, the sampling interval was less than 5 cm. Farther away, samples were collected on 10- to 20-cm intervals. Five background samples were also taken several meters above and below the boundary. Split samples were analyzed for trace elements by neutron activation at UCLA and by X-ray fluorescence (XRF) for major and minor elements at the Free University of Brussels. The data were then subjected to multivariate statistical analyses.

X-ray fluorescence

Major and minor element concentrations (Si, Al, Fe, Mg, Ca, Na, K, P, S) were determined by X-ray wavelength dispersive spectrometry on pure rock powder pellets using a 3 Kw Philipps PW 1404 with Rh-side window tube. Calibrations were performed with international shales and soils standards (SB0-1, PRI-1, AWI-1, SO-1, SO-3, TB, TS, SGR-1, MAG-1, SDC-1, BCSS-1; Govindaraju, 1989). The standard error of estimate (root mean square on regression) for this method ranges from 2 to 5% for SiO_2, Al_2O_3, Fe_2O_3 (total), and K_2O to about 10% for MgO, Na_2O, P_2O_5, and S at the average concentration of these elements in the Hony shales. CaO measurements must be considered as semiquantitative because of their low value (0.4 wt% on average) in the Hony shales.

Neutron activation

The samples analyzed by neutron activation were split into two subsamples. The first split sample batch was irradiated at the reactor facility of the University of Missouri (25 hrs at 7.6×10^{13} n cm^{-2} s^{-1}). Ir was measured following Ir purification using a radiochemical neutron activation procedure similar to that of Kyte et al., (1992). After counting, the Ir carrier recovery was determined by ICP-emission spectroscopy. Ir yields were all above 26%. The second batch of samples was irradiated for 5 hrs in the University of California, Riverside, reactor, which uses a neutron flux of 1.8×10^{-12} n cm^{-2} s^{-1}. Samples were then analyzed for trace elements (Sc, Cr, Co, Ni, Zn, As, Rb, Sb, Ce, Ba, La, Ce, Nd, Sm, Eu, Tb, Yb, Lu, Hf, Ta, Th, U) by instrumental neutron activation. The samples were counted on coaxial high-purity intrinsic Ge crystal gamma-ray detectors. Samples were counted twice; the first time the week following irradiation and then 3 weeks after irradiation. U.S.G.S. standard rock powders SCO-1 and BHVO-1 and a powder of Allende meteorite were analyzed in parallel.

INTERPRETATION OF RESULTS

Ir analyses

The analytical results are presented in Table 1, Fig. 3 and in the appendix. No significant positive Ir anomaly was detected in the 2 m of section investigated (Fig. 3). The interpretation of the one point precisely at the spherule layer, where Ir increases up to 83 pg/g over a background of about 40 pg/g, is uncertain. This increase may correspond to a small Ir anomaly of unknown origin, but considering analytical uncertainties, it is probably not significant at the two sigma level. Two similar spot increases occur, at 18 cm above the F/F boundary in the dark shale unit and in the basal Famennian shales (Fig. 3). The Hony Ir results demonstrate that there is no Ir anomaly comparable in magnitude to that observed at the K/T boundary. This conclusion is in agreement with previous Ir measurements at the F/F boundary in the nearby Sinsin section (McGhee et al., 1984; Orth et al., 1990). The absence of an anomaly invalidates the hypothesis that an Ir anomaly existed at the F/F boundary but had not been detected in Sinsin because of the missing interval.

Major element analyses

Table 1 shows that on average the Hony shale is comparable in composition to several reference shales. Nevertheless some differences are worth mentioning. The major oxide composition, depleted in SiO_2 and enriched in Al_2O_3, K_2O, and Fe_2O_3, demonstrates that the Hony shales are enriched in a clay-mineral component compared to the reference shales. This is in agreement with the sedimentological interpretation that the depositional setting of the shales was the outer shelf, well below wave base and distal to major sediment sources. Calcium carbonate content is much lower than in reference shales and is probably related to low oxygen conditions that restricted the abundance of carbonate-producing organisms in the depositional environment. Diagenetic remobilization of $CaCO_3$ from bioclasts and its reprecipitation as limestone nodules, found locally in the shales, may also account for the low CaO content of the Hony shales. On average, the S also appears low compared to the value for shelf shales (Wedepohl, 1969). However, S is rarely measured in shales, and the literature value may not accurately represent the true range of S abundance. In the Hony samples, S concentrations vary greatly from 47 ppm to 536 ppm.

Trace element analyses

Trace element compositions are in the range of reference shales from the literature and for most elements have low standard deviations (Table 1). Zinc and As are the only elements that show a significant enrichment compared to reference shales; they also have high standard deviations and larger range when compared to the other trace elements analyzed (Table 1, columns 3, 4). The olive-green shales are homogeneous in trace element composition, whereas there are some significant variations for the darker shale layers across the F/F boundary. When elemental composition is plotted against the stratigraphic column (Fig. 4), a distinct enrichment in S, Zn, As, and Sb appears localized over a 60- to 80-cm interval across the F/F boundary.

This increase in chalcophile elements begins in the gray shale unit, 20 to 50 cm below the base of the F/F boundary, culminates in the finer and darker shales above the F/F boundary, and abruptly terminates just under the limestone beds containing the first Famennian conodonts. The enrichment appears to correlate with a marked variation in shale color from olive-green in the Frasnian and Famennian to dark-gray near the boundary. The four elements seem to be correlated despite their sawtooth pattern, but the rise in As, Zn, and Sb predates that of the S by ≈30 cm.

Rare earth element (REE) abundances in samples of the Hony shales are comparable (Fig. 5) to those of the North American Shale Composite (Taylor and McLennan, 1985). The absence of Ce fractionation probably indicates (Fig. 5) that shelf waters were too reduced for Mn coatings to form or that they were redissolved by deeper low-oxygen water. Under ambient oceanic conditions, dissolved Ce is usually oxidated and incorporated in Mn and Fe coatings (Sholkovitz et al., 1994).

Factor analysis

The data were analyzed by factor analysis with the SPSS/PC$^+$ program (Norusis, 1991) to clarify the nature of the complex interactions between variables and to confirm the qualitative trend observed for chalcophile elements. The aim of factor analysis is to reduce observed relationships among several variables to more fundamental relationships among fewer, newly established variables, called factors. Theoretical and practical aspects of factor analyses in geology are described in details in Jörskog et al. (1976).

The results of the factor analysis are summarized in Figure 6. This figure presents the six factors that account for 80% of the total variance of major and trace elements in the Hony shales and the importance, or loading, of each element in each factor. This schematic representation identifies groups of coherent elements and provides clues to their genetic significance. Factor analysis demonstrates that the distribution of the elements is not subject to important random variations in the Hony shales. Ir is the only exception: Only 25% of its total vari-

TABLE 1. HONY SHALE COMPOSITION COMPARED TO REFERENCE SHALES*

	Average	Hony Shale Std. Dev.	Range	Terrigenous Shale†	Mean Shale§	NASC**	Shelf Shale‡
Oxides in wt. %							
SiO_2	50.0	2.9	43 to 54	59	55.4	58.3	50.7
Al_2O_3	20.1	1.1	18 to 22	17.7	16.5	15.2	15.1
Fe_2O_{3t}	8.0	1.1	6.2 to 11.4	6.6	7.2	5.5	6.7
MgO	2.0	0.2	1.6 to 2.7	2.1	2.4	2.6	3.3
CaO	0.4	0.03	0.35 to 0.45	1.2	3.8	3.2	7.2
Na_2O	0.6	0.07	0.46 to 0.74	1.1	1	1	0.8
K_2O	5.0	0.4	4.1 to 5.7	3.5	3.1	3.6	3.5
P_2O_5	0.12	0.01	0.11 to 0.17	0.15	0.2	0.1	0.1
S (ppm)	163	134	47 to 536	n.a.	n.a.	n.a.	2400
LOI	n.a.			6	≈10	≈10	≈12
Elements in ppm							
Sc	20.1	1	18 to 22	16	13	14.9	
Cr	117	6	109 to 128	110	90	124.5	
Co	20	9	8 to 57	23	19	25.7	
Ni	64	18	28 to 99	55	68	58	
Zn	164	103	74 to 459	85	95	n.a.	
As	39	15	14 to 66	n.a.	13	28.4	
Rb	185	14	150 to 206	160	140	125	
Sb	1.3	0.4	0.69 to 2.02	n.a.	1.5	2.1	
Cs	8.3	1.4	6.3 to 11.0	15	5	5.2	
Ba	448	41	345 to 532	650	580	636	
La	46	3	38 to 53	38	92	31.1	
Ce	82	6	72 to 95	80	59	66.7	
Nd	38	5	30 to 55	32	24	27.4	
Sm	5.9	0.9	4.5 to 8.6	5.6	6.4	5.6	
Eu	1.3	0.4	0.75 to 2.7	1.1	1	1.18	
Tb	0.71	0.19	0.42 to 1.35	0.77	1	0.85	
Yb	2.51	0.33	1.9 to 3.2	2.8	2.6	3.06	
Lu	0.38	0.04	0.30 to 0.45	0.43	0.7	0.46	
Hf	4.1	0.3	3.5 to 4.6	5	2.8	6.3	
Ta	1.24	0.07	1.1 to 1.4	n.a.	0.8	1.12	
Th	14.1	0.7	12.6 to 15.7	14.6	12	12.3	
U	2.4	0.2	2.8 to 2.0	3.1	3.7	2.66	
Ir (pg/g)	50	14	19 to 83.5	20	n.a.	n.a.	

*Average of 37 samples of Hony shales.
†Taylor and McLennan, 1985.
§Turekian and Wedepohl, 1961.
**Gromet et al., 1984.
‡Wedepohl, 1969.
For Turekian and Wedepohl, Gromet et al., and Wedepohl, major element recalculated assuming a loss on ignition (LOI) of 10 wt% (Turekian and Wedepohl and Gromet et al.) and 12 wt% for Wedepohl. n.a. = data not available.

ance is explained by the six factors identified in Fig. 6. The remaining 75% of Ir variance is specific to that element.

It is not the goal of this chapter to discuss in detail the geological significance of the six different factors indentified. This will be the topic of another paper presently in preparation. The discussion here will focus on factor 2 (Fig. 6), which confirms and reinforces the chalcophile trend already recognized in the dark-gray shale beds across the F/F boundary.

Factor 2 is highly loaded by a coherent chalcophile group formed by As, Sb, and Zn. It is less loaded by P_2O_5 and only weakly so by S, U, and Fe_2O_{3t}. Factor 2 explains all the variance of As and Sb, and most of that of Zn and P. Except for P_2O_5 and U, all the elements influencing factor 2 are chalcophiles and concentrate in reducing environments in the form of sulfides and/or are adsorbed on organic compounds (Vine and Tourtelot, 1970; Berner, 1971; Calvert, 1976). Uranium is commonly enriched in anoxic sediments (Calvert, 1976). This enrichment is mainly due to reduction of soluble U^{6+} to rela-

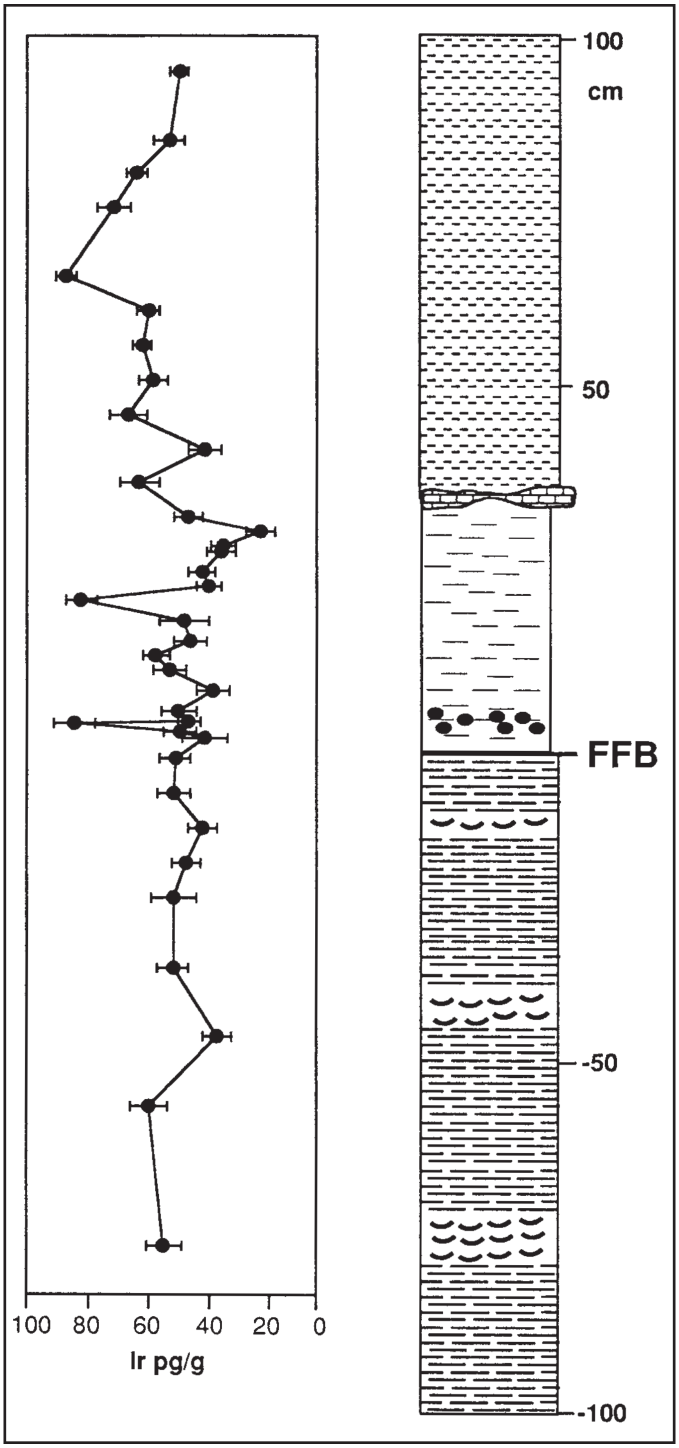

Figure 3. Ir profile across the studied interval. Error bar given at the 1 σ level. No significant Ir anomaly is associated with the spherule layer.

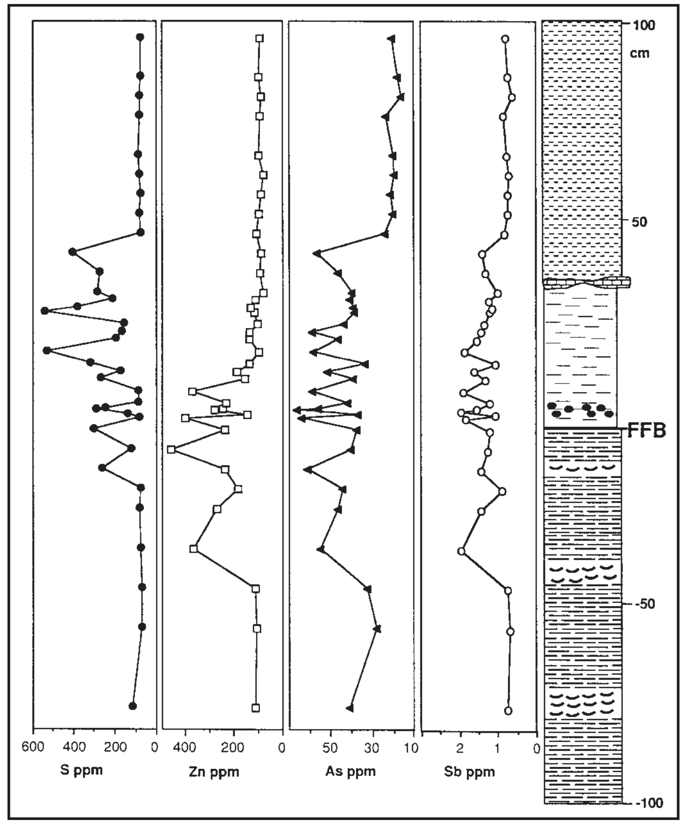

Figure 4. Profile of chalcophile elements (S, Zn, As, Sb) across the F/F boundary. The increase in chalcophiles begins in the gray shale bed, 20 to 50 cm below the boundary and culiminates in the dark shale bed just above the boundary. There is an abrupt return to normal shale content in chalcophile in basal Famennian shales. The increase in S, Zn, As, and Sb is interpreted to represent a significant decrease in oxygen conditions in the depositional environment.

tively insoluble U^{4+} (Klinkhammer and Palmer, 1991). The low U concentration (Table 1) and the weak saturation of factor 2 by U (Fig. 6) show that the depositional environment was dysoxic to suboxic (Tyson and Pearson, 1991) or that the sedimentation rate was too high for significant fixation of U to take place (Jones and Manning, 1994). The variance of U is mainly controlled by factor 1, which is interpreted to represent a global terrigenous-absorption clay factor. Phosphorus loading is probably due to P association with organic matter preserved in suboxic environments. The weak loading by Fe_2O_{3t} and S may indicate the sporadic occurrence of early diagenetic pyrite. Factor 2 can thus be interpreted as representing paleoredox conditions in the depositional environment.

The weak negative loading of factor 2 by Ba, Ir, Rb, and Yb (Fig. 6) may be due to a limited negative correlation between factor 2 and factor 1. These negative loadings must be considered an artifice induced by the use of an orthogonal instead of an oblique model for the factor rotation. They have no effect on the interpretation of factor 2.

The 2 m of F/F boundary section investigated in Hony appears to be characterized by generally limited oxygen conditions, as illustrated by the olive-green color of the shales and the local presence of rare pyrite crystals. Figure 7 shows the variation of factor 2 scores, representing a quantitative estimation of the reducing character of the depositional environment

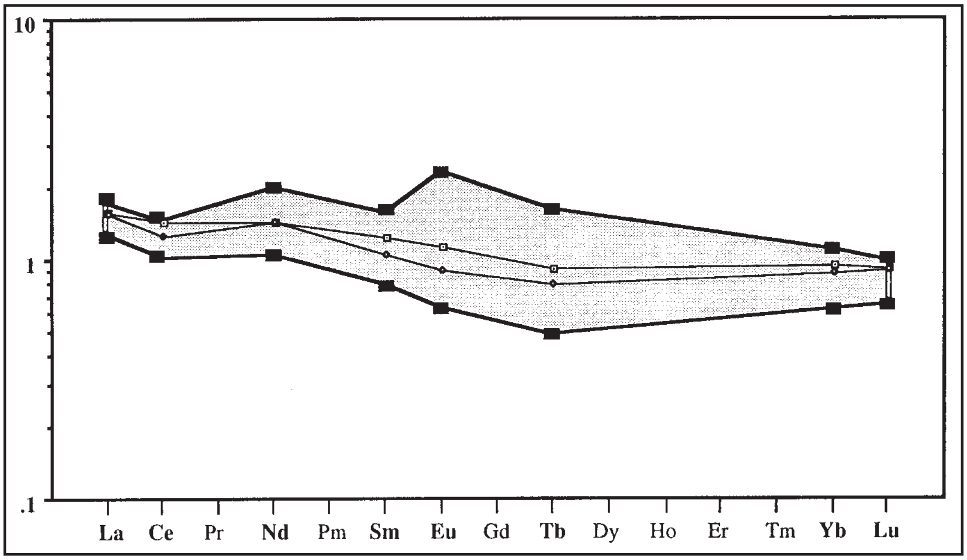

Figure 5. Range of rare earth elements normalized to the North American Shale Composite (NASC) (Gromet et al., 1984). The pattern is flat, indicating the similarity between the Hony shales and NASC. No Ce anomaly is present. Only the eight elements in boldface type were analyzed. The open squares represent a sample from the dark shales at the boundary, the diamonds a sample from the olive-green Famennian shales.

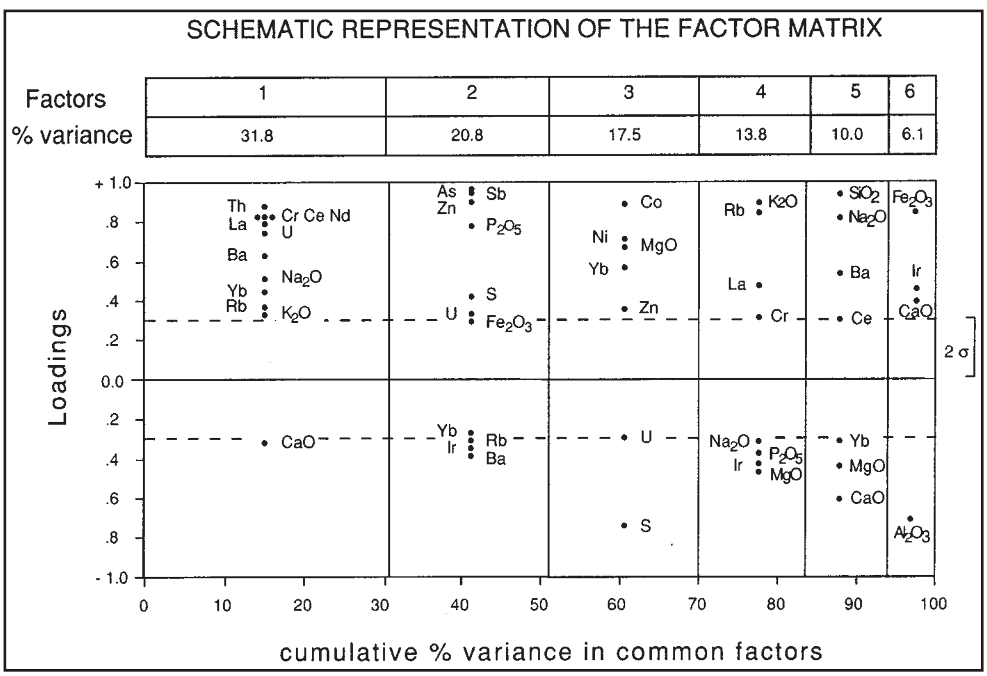

Figure 6. Schematic representation of the varimax factor matrix. Number of elements (variables): 24; number of samples: 37. Variables were $\log_{10}$ transformed, and this figure presents the simple structure obtained by orthogonal rotation using the varimax criteria (Norusis, 1991). The width of the rectangles is proportional to the variance of each factor. The dots represent the load of each element in each factor. Loadings below 0.3 are insignificant and not shown here. Factor 2 is heavily loaded with chalcophile elements and is interpreted to indicate reducing conditions in the depositional environment.

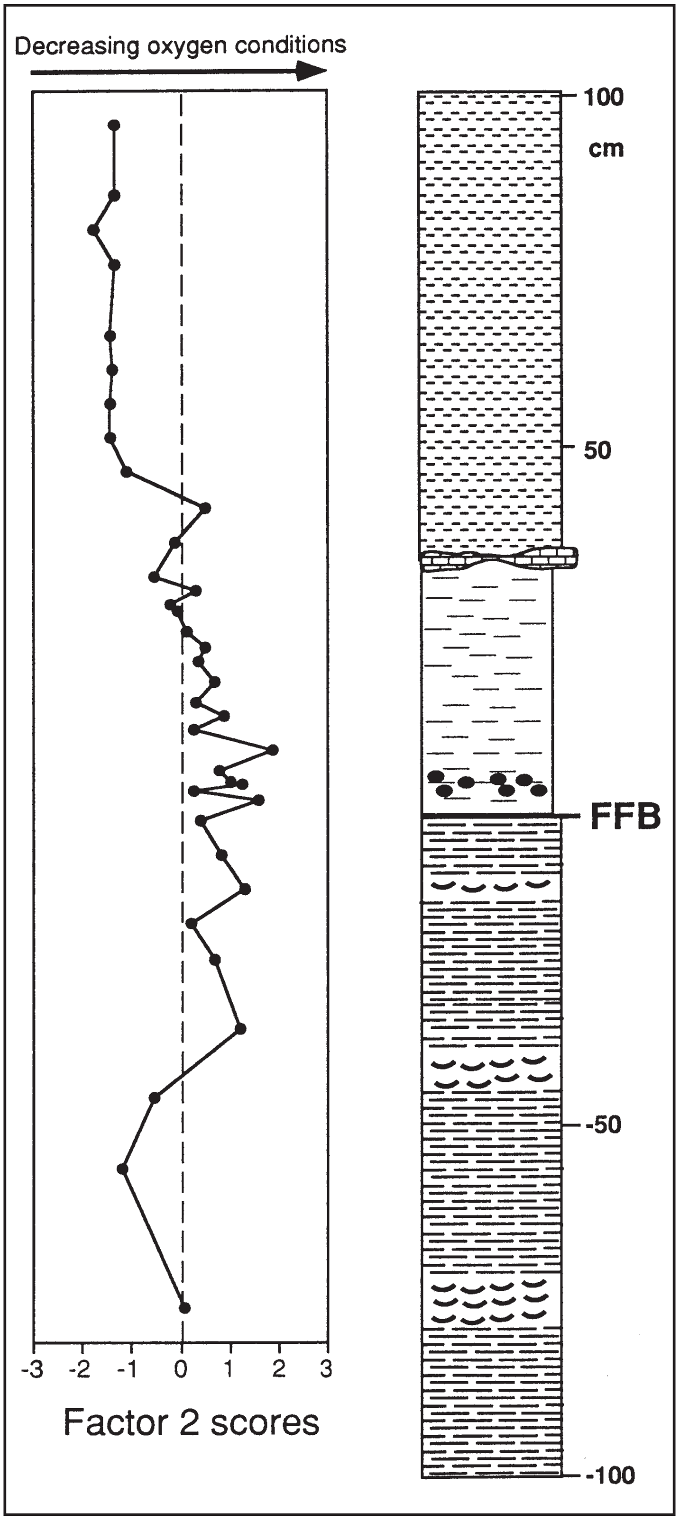

Figure 7. Factor 2 scores profile across the F/F boundary. The scores are presented in standardized values and represent the influence and intensity of factor 2 on each sample. Factor 2 is interpreted to represent reducing conditions in the depositional environment. Factor 2 scores quantatively confirm the reducing trend visible in Figure 4; more intense reducing conditions are in the dark shale bed above the F/F boundary.

for each sample across the F/F boundary. A 70 cm interval right at the boundary is marked by a net increase in low oxygen conditions (Figs. 4 and 7). This increase begins 10 to 20 cm below the F/F boundary and is most intense in the 40-cm, fine, dark, shale bed overlying the boundary. The overlying Famennian is marked by a rapid return to more oxygenated conditions.

DISCUSSION

No Ir anomaly comparable in magnitude to that of the K/T boundary was detected in the Hony section associated with the F/F boundary and microtektite-like spherule layer. The interpretation of the very minor Ir increase found in the spherule remains unclear and inconclusive. As in the Cenozoic, microtektite events do not seem to be associated with major Ir anomalies (Glass, 1990). The rare occurence of Ir anomalies associated with impact events in the sedimentary record was reviewed by Kyte (1988). A small peak in Ir (190 pg/g or ≈2 × the continuum level) has recently been identified in Ocean Drilling Project (ODP) core 758 B from the Ninetyeast Ridge, eastern Indian Ocean, associated with the 0.77-Ma Australasian microtektite strewnfield (Schmidt et al., 1993). In the Late Devonian, the Chinese microtektites apparently coincide with a 300 pg/g Ir anomaly in the Canning Basin in Australia (Wang, 1992). This Ir anomaly had been tentatively interpreted to have been induced by Ir concentration from seawater by *Frutexites* algae (Playford et al., 1984). This Ir peak is higher than that corresponding to the Australasian tektite event and suggests that the Famennian Canning Basin Ir anomaly is related to the impact that produced the Chinese microtektites. These Ir anomalies are more than an order of magnitude below the Ir level detected at the K/T boundary (Alvarez et al., 1980; Kyte et al., 1980) and in sediments recording a late Pliocene impact event in the southern Ocean (Kyte et al., 1988).

Trace element analyses combined with factor analysis in the Hony section indicate a change from oxygen-limited to dysaerobic or perhaps even anoxic conditions at the F/F boundary. Such a change can be caused by a rise of the oxygen minimum zone in the paleo-Tethys ocean and subsequent overflow of oxygen-depleted waters onto the shallow shelf environment. During the late Paleozoic, the paleo-Tethys ocean was probably strongly oxygen-stratified. Low oxygen conditions appear widespread in the paleo-Tethys at the F/F boundary (Buggisch, 1991). There is evidence of low-oxygen conditions at this stratigraphic level in the Canadian Rocky Mountains (Geldsetzer et al., 1987) and perhaps in south China (Wang et al., 1991). Joachimski and Buggisch (1993) described positive $\delta^{13}C$ anomalies indicative of anoxic depositional conditions just below the F/F boundary in the Coumiac (France) and Steinbruch Schmidt (Germany) sections. These anomalies coincide with the deposition of black limestones and shales in the upper Frasnian, known in Germany as the upper Kellwasser horizons. The anoxic Kellewasser horizons so far have not been identified in the Hony section. This study demonstrates that in Hony the F/F boundary is also characterized by an abrupt input of poorly oxygenated waters into shallow marine environments. This event seems less developed or perhaps less intense than in the Coumiac or Schmidt sections, as no truly anoxic or organic-rich bituminous facies formed in Hony. The development of anoxic conditions in the paleo-Tethys appears to vary according to local paleogeography, paleodepths, and paleoceanography.

The exact location of minimum oxygen conditions located in the bed of fine dark shales just above where Sandberg et al., (1988) have placed the boundary diverge between the Hony section and other F/F boundary sections in Western Europe. In other European sections low oxygen conditions are restricted to the upper Frasnian (Joachimski and Buggisch, 1993). This divergence may be due to the 1.5-m interval (Fig. 2) which lacks the detailed conodont biostratigraphy necessary to exactly locate the F/F boundary. The first appearence of Famennian conodonts is 35 cm above the F/F boundary in the first limestone bed topping this oxygen-depleted, dark-gray shale. The microtektite-like spherule layer coincides with the lowest oxygen conditions and occurs at the very base of this dark-gray shale bed (Claeys and Casier, 1994).

Anoxic conditions in the upper Frasnian have been hypothesized to be responsible for the extinction of organisms at the F/F boundary (Becker et al., 1991). This oxygen reduction may be related to rapid changes in sea level occurring at the boundary (Johnson et al., 1985; Sandberg et al., 1988; Becker et al., 1989). Both or either of these factors can potentially stress shallow marine organisms, in particular the large coral-stromatoporoid reefs, and lead to their disappearance. However, these factors are less likely to affect pelagic and deeper-water organisms.

The mechanisms causing these worldwide rapid sea-level fluctuations and changes in ocean chemistry have not yet been documented in detail. It is also unclear at this point how stratigraphically localized anoxic events like the Kellewasser horizons can explain the apparently stepwise extinction pattern over a time frame significantly longer than the brief anoxic periods. According to McGhee (1989), the extinction occurs over six conodont zones across the boundary.

The role of impact event(s) in the mass extinction is also unclear. Two impacts appear to have taken place within a few m.y. of the F/F boundary. Impact products in the form of microtektite-like glass particles have been identified in south China (Wang, 1992) and at two sites in Belgium (Claeys et al., 1992; Claeys and Casier, 1994). The Chinese spherules occur roughly 1.5 to 2 m.y. after the F/F boundary and coincide with a small Ir anomaly in the Canning Basin in Australia (Wang, 1992). At this point, neither of the two impact events appears to have a global distribution. Claeys and Casier (1994) have suggested that the Belgian glass spherules originated from the Siljan Ring impact structure in Sweden. This 54-km impact crater is unlikely to have had an effect comparable in magnitude to that of the much larger K/T boundary Chicxulub crater in Yucatan. On the other hand, the existence of two impacts within 1 to 2 m.y. perhaps suggests that at F/F time the Earth was bombarded by a comet shower (Hut et al., 1987). A hypothetical large oceanic impact could have taken place in the uppermost Frasnian, triggering mass extinctions, altering oceanic circulation, and raising the oxygen minimum zone in the ocean. If this was the case, tsunami deposits might be expected in the uppermost Frasnian. However, no strong evidence for tsunami deposits has so far been reported. Another hypothesis is that a succession of small impacts could induce local or global extinction of species if it coincided with a time when the shallow seas were already under severe anoxic stress. At this point, these scenarios remain purely speculative.

The relationships between possible impact event(s) taking place at or near the F/F boundary, the suboxic events, and the mass extinction need to be further clarified by paleontological, sedimentological, and geochemical studies. This may be a difficult task. The biostratigraphic resolution available for the Late Devonian (one conodont zone ≈0.5 Ma according to Ziegler and Sandberg, 1990), difficulties in worldwide correlations, and the restricted number of F/F boundary sections strongly limit the stratigraphic and temporal resolution that can be attained in the Late Devonian.

CONCLUSIONS

1. No Ir anomaly is associated with the F/F boundary or microtektite-like glass in the Hony section in Belgium. The lack of a positive Ir anomaly in Hony indicates that this impact differed, perhaps in magnitude or type of bolide, from the K/T boundary event and appears more similar to the four tektite-producing impacts that took place in the Cenozoic.

2. There is evidence in Hony of dysaerobic conditions at the F/F boundary. The Hony dark gray shales correlate with the upper Kellwasser anoxic event and further support the general anoxic trend identified at the F/F boundary at several other sites in the paleo-Tethys.

ACKNOWLEDGMENTS

This study was mainly funded by National Science Foundation grant EAR-9118701 to F. T. Kyte at UCLA. P. Claeys also acknowledges support from NASA grant NAGW-3008 and National Science Foundation grant EAR-91-05297 to W. Alvarez at UC Berkeley. A. Herbosch thanks the Belgian Fonds National de la Recherche Scientifique for a travel grant and J. L. Schlachmulder for help with the factor analyses. J-G. Casier and A. Herbosch are supported by a FRFC grant from the Fonds National de la Recherche Scientifique. The authors thank F. Asaro and B. Bohor for careful review and comments, which greatly improved this manuscript.

APPENDIX. NEUTRON ACTIVATION DATA

		SiO2	Al2O3	Fe2O3	MgO	CaO	Na2O	K2O	P2O5	S	Sc
Sample No	Distance glass	wt%	wt%	wt%	wt%	wt%	wt%	wt%	wt%	ug/g	ug/g
92-Ho-25	75 cm below	52.4	19.6	7.7	2.1	0.4	0.7	4.9	0.2	92.0	20.8
92-Ho-25’	55 cm below	52.6	19.7	7.5	2.1	0.4	0.7	4.8	0.1	47.0	20.1
92-Ho-25”	45 cm below	53.3	19.3	7.8	2.2	0.4	0.7	4.7	0.1	49.0	20.6
92-Ho-25”’	35 cm below	51.7	19.3	8.1	2.2	0.4	0.7	4.7	0.1	51.0	20.7
92-Ho-26	25 cm below	52.8	19.1	7.8	2.1	0.4	0.7	4.5	0.1	61.0	20.7
92-Ho-26’	20 cm below	53.0	19.6	9.1	2.1	0.4	0.7	4.7	0.1	54.0	20.6
92-Ho-26”	15 cm below	51.6	21.3	6.6	1.9	0.4	0.7	4.4	0.1	248.0	18.5
92-Ho-26”’	10 cm below	50.7	19.9	7.7	1.8	0.4	0.7	5.5	0.1	102.0	20.1
93-Ho-01	5 cm below	51.3	21.3	7.9	2.1	0.4	0.7	4.8	0.1	290.0	19.6
92-Ho-26””	2 cm below	46.2	21.9	7.8	2.0	0.4	0.5	5.6	0.1	58.0	19.3
92-Ho-27	1 cm below	43.4	18.4	9.4	2.1	0.4	0.6	5.6	0.1	118.0	21.0
93-Ho-02	0 cm	52.4	19.5	8.5	1.8	0.4	0.7	4.3	0.1	275.0	18.6
93-Ho-03	0 cm	50.8	21.2	7.0	1.7	0.4	0.7	4.9	0.1	230.0	20.6
93-Ho-04	2 cm above	50.1	20.8	7.7	1.9	0.4	0.6	5.4	0.1	66.0	20.7
93-Ho-05	5 cm above	48.7	18.7	11.4	1.9	0.4	0.5	5.4	0.1	67.0	20.8
92-Ho-27’	8 cm above	43.5	19.7	8.4	2.7	0.5	0.5	4.1	0.1	253.0	20.5
93-Ho-06	10 cm above	49.5	21.2	7.6	2.0	0.4	0.6	4.6	0.1	152.0	18.9
93-Ho-07	12 cm above	47.2	18.2	10.3	2.0	0.4	0.6	5.4	0.1	307.0	20.3
93-Ho-08	15 cm above	48.8	19.3	10.0	1.9	0.5	0.5	4.5	0.1	523.0	19.0
92-Ho-27”	18 cm above	46.3	20.0	9.5	2.4	0.5	0.5	4.5	0.1	179.0	21.3
93-Ho-09	20 cm above	46.1	20.7	7.5	2.2	0.5	0.6	4.8	0.1	148.0	19.3
93-Ho-10	22 cm above	50.3	21.4	8.2	1.8	0.4	0.6	5.2	0.1	136.0	20.3
93-Ho-11	25 cm above	44.7	21.0	6.2	2.1	0.4	0.5	5.5	0.1	536.0	21.6
93-Ho-12	26 cm above	53.6	20.0	7.0	1.7	0.4	0.6	5.3	0.1	373.0	18.8
92-Ho-27”’	28 cm above	53.5	21.8	6.6	1.8	0.4	0.5	5.1	0.1	193.0	19.9
93-Ho-13	30 cm above	50.5	21.0	7.9	1.6	0.4	0.6	5.7	0.1	270.0	21.6
93-Ho-14	35 cm above	49.1	20.1	8.5	1.6	0.4	0.6	5.4	0.1	257.0	21.4
92-Ho-28	40 cm above	50.1	21.3	8.0	1.7	0.4	0.6	5.1	0.1	392.0	20.7
93-Ho-15	45 cm above	45.2	20.5	7.4	2.1	0.4	0.6	5.4	0.1	51.0	20.3
93-Ho-16	50 cm above	51.4	20.3	6.9	2.0	0.4	0.6	5.1	0.1	59.0	20.4
92-Ho-28’	55 cm above	54.3	20.3	7.7	1.9	0.4	0.6	4.9	0.1	55.0	17.6
93-Ho-17	60 cm above	50.4	20.4	7.4	2.0	0.5	0.6	5.1	0.1	60.0	19.1
92-Ho-28”	65 cm above	51.7	20.0	8.4	2.0	0.4	0.6	5.1	0.1	66.0	20.2
93-Ho-18	75 cm above	49.7	20.6	7.7	2.1	0.4	0.6	4.9	0.1	56.0	19.4
92-Ho-28”’	80 cm above	50.7	19.5	8.2	2.0	0.4	0.6	5.1	0.1	56.0	20.2
92-Ho-29	85 cm above	51.8	20.1	8.0	2.1	0.4	0.6	4.8	0.1	54.0	20.2
93-H0-19	95 cm above	51.1	18.2	6.8	2.1	0.4	0.6	4.9	0.1	52.0	20.4
92-Ho-02 BG	6 M below	nd	nd	nd	nd	nd	nd	nd	nd	nd	17.2
92-Ho-14 BG	3 M below	nd	nd	nd	nd	nd	nd	nd	nd	nd	18.8
92-Ho-37 BG	4 M above	nd	nd	nd	nd	nd	nd	nd	nd	nd	4.2
92-Ho-40 BG	6 M above	nd	nd	nd	nd	nd	nd	nd	nd	nd	19.9
93-Ho-20 BG	15 M above	nd	nd	nd	nd	nd	nd	nd	nd	nd	19.2
SCO-1		nd	nd	nd	nd	nd	nd	nd	nd	nd	11.5
BHVO		nd	nd	nd	nd	nd	nd	nd	nd	nd	29.9
Allende		nd	nd	nd	nd	nd	nd	nd	nd	nd	nd

APPENDIX. NEUTRON ACTIVATION DATA

		Cr	**Co**	**Ni**	**Zn**	**As**	**Rb**	**Sr**	**Sb**	**Cs**	**Ba**
Sample No	Distance glass	ug/g	ug/g	ug/g	ug/g	ug/g	ug/g	ug/g	ug/g	ug/g	ug/g
92-Ho-25	75 cm below	120.3	23.3	68.7	108.0	39.6	185.6	91.1	0.8	10.5	483.4
92-Ho-25’	55 cm below	112.6	12.6	75.1	101.4	26.0	180.3	86.3	0.8	9.6	532.1
92-Ho-25”	45 cm below		16.7	62.2	107.8	30.4	180.9	121.2	0.8	9.7	498.2
92-Ho-25”’	35 cm below	117.6	57.0	99.3	366.7	54.1	177.3	109.7	2.0	10.8	513.8
92-Ho-26	25 cm below	116.0	35.3	54.8	270.3	45.6	178.2	<82.5	1.5	8.6	493.1
92-Ho-26’	20 cm below	119.2	27.3	75.7	182.6	43.1	181.8	98.0	1.0	8.7	486.0
92-Ho-26”	15 cm below	111.5	16.5	67.7	237.0	60.5	163.8	86.2	1.5	6.5	414.9
92-Ho-26”’	10 cm below	123.1	18.9	54.0	459.4	39.0	202.0	170.9	1.3	7.5	450.0
93-Ho-01	5 cm below	118.8	10.2	34.8	236.5	35.7	173.6	<111.8	1.3	7.8	483.1
92-Ho-26””	2 cm below	112.4	20.4	52.2	403.7	63.7	189.2	<101.6	1.9	9.7	381.3
92-Ho-27	1 cm below	127.7	18.6	43.9	144.3	35.2	202.5	127.1	1.1	7.5	444.7
93-Ho-02	0 cm	108.5	13.2	76.8	279.9	65.7	154.3	<124.0	2.0	6.3	434.8
93-Ho-03	0 cm	120.0	13.4	74.5	243.4	55.2	179.4	<82.6	1.6	7.3	447.3
93-Ho-04	2 cm above	126.6	24.7	74.3	231.7	40.7	205.8	154.8	1.3	8.1	469.3
93-Ho-05	5 cm above	120.3	25.3	91.2	373.0	58.0	200.9	98.7	2.0	11.0	409.7
92-Ho-27’	8 cm above	112.9	20.3	100.3	151.2	37.5	150.3	<88.6	1.4	6.7	344.8
93-Ho-06	10 cm above	109.5	26.2	79.6	186.6	50.5	172.0	<82.7	1.7	7.8	374.2
93-Ho-07	12 cm above	124.8	12.3	55.6	131.0	31.9	194.9	<80.3	1.1	7.1	428.8
93-Ho-08	15 cm above	109.7	12.1	27.9	94.1	57.6	159.3	161.2	1.9	6.3	413.6
92-Ho-27”	18 cm above	118.1	24.8	62.0	132.3	45.3	166.8	123.9	1.6	7.5	392.7
93-Ho-09	20 cm above	109.0	19.4	83.5	130.1	58.0	174.3	<65.3	1.5	7.3	378.2
93-Ho-10	22 cm above	117.9	16.9	55.9	98.4	42.1	194.5	95.4	1.4	7.8	442.5
93-Ho-11	25 cm above	126.5	12.5	46.4	112.7	37.0	196.2	77.4	1.3	9.3	467.5
93-Ho-12	26 cm above	108.9	8.9	<35.5	129.1	37.8	183.2	103.1	1.2	6.6	416.0
92-Ho-27”’	28 cm above	109.0	14.2	76.0	106.7	39.4	189.0	<67.2	1.3	7.2	422.8
93-Ho-13	30 cm above	120.2	15.6	56.1	73.4	38.1	198.9	93.5	1.1	7.0	482.6
93-Ho-14	35 cm above	126.0	7.6	34.2	86.1	45.1	197.5	83.0	1.4	6.5	481.2
92-Ho-28	40 cm above	117.3	14.0	54.8	81.2	56.1	178.5	<56.6	1.5	6.7	430.1
93-Ho-15	45 cm above	119.4	21.9	42.5	101.5	21.7	194.6	74.6	0.9	10.3	481.9
93-Ho-16	50 cm above	115.8	19.3	66.4	91.5	17.8	199.7	113.5	0.8	8.2	451.6
92-Ho-28’	55 cm above	109.9	16.5	56.8	84.9	18.7	190.9	86.5	0.8	8.6	467.5
93-Ho-17	60 cm above	109.5	26.7	87.1	74.5	17.1	184.9	<53.9	0.8	10.3	443.0
92-Ho-28”	65 cm above	118.4	17.3	65.1	92.5	17.9	197.8	75.5	0.8	8.2	453.7
93-Ho-18	75 cm above	109.5	28.6	45.6	88.8	21.1	180.6	85.5	0.9	10.0	467.8
92-Ho-28”’	80 cm above	115.8	15.6	48.0	84.4	13.6	194.2	99.5	0.7	9.1	466.7
92-Ho-29	85 cm above	114.9	20.0	71.3	91.2	15.1	192.3	77.2	0.8	10.0	435.6
93-H0-19	95 cm above	116.8	21.6	73.9	90.3	18.3	191.8	72.0	0.9	10.4	487.9
92-Ho-02 BG	6 M below	110.3	22.1	64.4	74.4	12.4	165.9	113.0	0.8	8.3	787.6
92-Ho-14 BG	3 M below	106.4	22.7	49.0	108.5	6.9	182.0	114.4	1.1	10.4	526.3
92-Ho-37 BG	4 M above	8.0	11.2	24.1	25.1	9.7	14.1	449.4	0.6	3.0	76.1
92-Ho-40 BG	6 M above	113.8	21.1	71.5	82.3	11.9	205.6	105.1	1.0	13.3	429.0
93-Ho-20 BG	15 M above	110.9	17.6	78.9	71.0	12.8	198.3	113.8	0.9	11.5	398.3
SCO-1		69.0	11.0	26.1	94.1	10.9	104.9	181.3	2.4	7.4	527.8
BHVO		275.4	43.2	114.1	102.8	<1.1	13.5	365.8	0.2	<0.2	122.1
Allende		nd	nd	nd	nd	nd	nd	nd	nd	nd	nd

APPENDIX. NEUTRON ACTIVATION DATA

		La	Ce	Nd	Sm	Eu	Tb	Yb	Lu	Hf	Ta
Sample No	Distance glass	ug/g	ug/g	ug/g	ug/g	ug/g	ug/g	ug/g	ug/g	ug/g	ug/g
92-Ho-25	75 cm below	47.9	88.9	41.9	6.9	1.4	0.9	2.9	0.4	4.3	1.3
92-Ho-25’	55 cm below	47.5	85.5	55.1	7.6	1.6	0.9	2.8	0.4	4.1	1.2
92-Ho-25”	45 cm below	49.6	90.0	40.8	6.7	1.4	0.9	2.8	0.4	4.6	1.2
92-Ho-25”’	35 cm below	48.5	95.6	39.2	6.9	1.3	0.8	2.9	0.4	4.2	1.2
92-Ho-26	25 cm below	46.2	85.9	40.4	6.7	1.3	0.9	3.0	0.5	4.2	1.2
92-Ho-26’	20 cm below	48.1	87.2	43.0	6.0	1.1	0.8	2.8	0.4	4.2	1.3
92-Ho-26”	15 cm below	41.6	75.3	35.9	4.7	0.9	0.5	2.0	0.3	4.0	1.1
92-Ho-26”’	10 cm below	47.2	83.8	39.3	7.2	1.7	0.8	2.6	0.4	3.8	1.2
93-Ho-01	5 cm below	49.5	85.9	40.3	5.8	1.1	0.7	2.6	0.4	4.5	1.3
92-Ho-26””	2 cm below	48.3	82.1	38.7	6.1	1.4	0.7	2.4	0.4	3.7	1.2
92-Ho-27	1 cm below	50.9	88.9	46.2	6.7	1.5	0.7	2.4	0.4	4.8	1.4
93-Ho-02	0 cm	42.3	76.3	31.1	4.8	0.8	0.4	2.0	0.3	4.5	1.1
93-Ho-03	0 cm	43.8	77.4	35.7	5.1	1.0	0.5	2.1	0.3	4.1	1.2
93-Ho-04	2 cm above	46.5	82.5	37.4	5.5	1.0	0.5	2.1	0.3	3.8	1.3
93-Ho-05	5 cm above	48.7	84.0	38.1	6.2	1.3	0.6	2.4	0.3	3.8	1.2
92-Ho-27’	8 cm above	37.6	67.1	31.4	7.4	2.2	1.2	3.1	0.4	3.7	1.2
93-Ho-06	10 cm above	43.6	76.6	32.7	5.3	1.0	0.6	2.3	0.4	4.1	1.2
93-Ho-07	12 cm above	49.2	84.1	36.9	6.0	1.3	0.6	2.5	0.4	4.8	1.4
93-Ho-08	15 cm above	47.4	77.2	41.0	5.5	1.3	0.6	2.2	0.3	4.2	1.1
92-Ho-27”	18 cm above	43.3	72.3	29.8	8.6	2.7	1.3	3.2	0.4	4.1	1.2
93-Ho-09	20 cm above	44.0	72.4	35.4	7.1	2.3	1.1	2.4	0.4	3.8	1.2
93-Ho-10	22 cm above	46.1	76.8	32.4	5.9	1.6	0.7	2.2	0.3	3.8	1.3
93-Ho-11	25 cm above	48.2	75.7	40.3	5.3	1.3	0.6	2.3	0.4	4.2	1.3
93-Ho-12	26 cm above	44.7	74.0	29.5	4.5	1.0	0.4	1.9	0.3	3.7	1.2
92-Ho-27”’	28 cm above	44.3	73.0	30.4	5.1	1.3	0.6	2.1	0.3	3.5	1.1
93-Ho-13	30 cm above	48.2	86.6	41.1	5.1	0.9	0.6	2.6	0.4	4.2	1.4
93-Ho-14	35 cm above	53.2	95.0	48.3	5.5	0.8	0.6	2.5	0.4	4.5	1.4
92-Ho-28	40 cm above	48.1	86.1	39.1	4.8	0.8	0.7	2.6	0.4	4.2	1.3
93-Ho-15	45 cm above	47.0	83.4	37.3	6.0	1.2	0.8	2.8	0.4	4.4	1.3
93-Ho-16	50 cm above	47.2	82.8	39.5	5.4	1.0	0.7	2.7	0.4	4.4	1.2
92-Ho-28’	55 cm above	42.4	75.3	35.2	5.0	0.9	0.5	2.1	0.3	4.2	1.2
93-Ho-17	60 cm above	44.2	81.3	33.9	5.7	1.1	0.8	2.5	0.4	3.8	1.2
92-Ho-28”	65 cm above	47.9	84.0	39.5	5.8	1.1	0.7	2.7	0.4	4.1	1.3
93-Ho-18	75 cm above	44.5	78.6	36.9	5.3	1.0	0.7	2.7	0.4	3.9	1.2
92-Ho-28”’	80 cm above	46.9	82.9	37.6	5.3	1.1	0.7	2.6	0.4	4.2	1.3
92-Ho-29	85 cm above	46.2	82.4	36.3	5.6	1.1	0.8	2.7	0.4	4.2	1.3
93-H0-19	95 cm above	46.0	80.9	34.6	5.4	1.0	0.7	2.6	0.4	4.3	1.3
92-Ho-02 BG	6 M below	44.8	79.7	32.6	5.4	1.1	0.7	2.5	0.4	4.5	1.0
92-Ho-14 BG	3 M below	42.7	78.1	30.8	6.1	1.3	0.7	2.5	0.4	3.9	1.1
92-Ho-37 BG	4 M above	9.4	25.8	19.9	6.0	1.9	0.8	1.2	0.2	0.3	0.1
92-Ho-40 BG	6 M above	44.1	76.9	34.5	5.1	1.0	0.7	2.3	0.4	3.4	1.1
93-Ho-20 BG	15 M above	44.7	77.4	35.1	5.4	1.0	0.7	2.4	0.4	3.8	1.0
SCO-1		29.5	49.7	28.5	4.6	1.1	0.7	2.2	0.3	4.4	0.7
BHVO		14.9	32.0	23.1	5.4	2.0	0.9	1.9	0.3	4.0	1.0
Allende		nd	nd	nd	nd	nd	nd	nd	nd	nd	nd

APPENDIX. NEUTRON ACTIVATION DATA

Sample No	Distance glass	Th ug/g	U ug/g	Ir pg/g
92-Ho-25	75 cm below	14.7	2.6	52.6
92-Ho-25’	55 cm below	13.8	2.4	57.9
92-Ho-25”	45 cm below	14.5	2.4	34.5
92-Ho-25’”	35 cm below	14.2	2.3	49.6
92-Ho-26	25 cm below	14.3	2.4	49.4
92-Ho-26’	20 cm below	14.2	2.4	45.0
92-Ho-26”	15 cm below	13.9	2.5	39.2
92-Ho-26’”	10 cm below	14.1	2.4	49.4
93-Ho-01	5 cm below	14.5	2.7	48.9
92-Ho-26””	2 cm below	13.3	2.3	38.5
92-Ho-27	1 cm below	15.5	2.4	47.2
93-Ho-02	0 cm	13.7	2.6	83.5
93-Ho-03	0 cm	14.4	2.6	44.1
93-Ho-04	2 cm above	14.0	2.5	47.7
93-Ho-05	5 cm above	13.7	2.4	36.0
92-Ho-27’	8 cm above	12.8	2.2	50.6
93-Ho-06	10 cm above	14.1	2.2	55.4
93-Ho-07	12 cm above	15.4	2.5	43.8
93-Ho-08	15 cm above	13.5	2.5	45.8
92-Ho-27”	18 cm above	13.8	2.3	81.4
93-Ho-09	20 cm above	13.0	2.0	37.1
93-Ho-10	22 cm above	13.9	2.2	39.6
93-Ho-11	25 cm above	14.7	2.6	33.2
93-Ho-12	26 cm above	13.0	2.0	32.3
92-Ho-27’”	28 cm above	12.6	2.1	19.3
93-Ho-13	30 cm above	14.9	2.5	44.2
93-Ho-14	35 cm above	15.7	2.8	61.2
92-Ho-28	40 cm above	15.1	2.6	38.5
93-Ho-15	45 cm above	14.5	2.3	65.0
93-Ho-16	50 cm above	14.0	2.4	56.3
92-Ho-28’	55 cm above	13.7	2.2	60.3
93-Ho-17	60 cm above	13.3	2.1	58.2
92-Ho-28”	65 cm above	14.3	2.2	86.5
93-Ho-18	75 cm above	13.3	2.2	69.9
92-Ho-28’”	80 cm above	14.0	2.3	62.2
92-Ho-29	85 cm above	13.9	2.3	51.1
93-H0-19	95 cm above	14.0	2.3	47.4
92-Ho-02 BG	6 M below	12.1	2.4	59.5
92-Ho-14 BG	3 M below	13.6	2.0	62.7
92-Ho-37 BG	4 M above	1.9	0.6	15.7
92-Ho-40 BG	6 M above	12.9	2.0	59.4
93-Ho-20 BG	15 M above	12.7	1.9	63.7
SCO-1		8.8	2.7	nd
BHVO		1.1	0.5	nd
Allende		nd	nd	189.5

REFERENCES CITED

Alvarez, L. W., Alvarez, W., Asaro, F., and Michel, H. V., 1980, Extraterrestrial causes for the Cretaceous-Tertiary extinction: Science, v. 208, p. 1095–1108.

Becker, T. R., Feist, R., Flajs, G., House, M. R., and Klapper G., 1989, Frasnian-Famennian extinction events in the Devonian at Coumiac France: Comptes Rendus Académie des Sciences de Paris, t. 309, ser. 2, p. 259–266.

Becker, T. R., House, M. R., Kirchgasser, W. T., and Playford, P. E., 1991, Sedimentary and faunal changes across the Frasnian-Famennian boundary in the Canning Basin of Western Australia: Historical biology, v. 5, p. 183–196.

Berner, R. A., 1971, Principles of chemical sedimentology: New York, McGraw Hill, 240 p.

Buggisch, W., 1991, The global Frasnian-Famennian Kellwasser event: Geologische Rundschau, v. 80, p. 49–72.

Calvert, S. E., 1976, The mineralogy and geochemistry of near-shore sediments. *in* Riley, J. R., and Chester, R., eds., Chemical Oceanography, Volume 6: New York, Academic Press, 187 p.

Casier, J.-G., and Devleeschouwer, X., 1994, Ostracods and the Upper Devonian mass extinction in the southern border of the Dinant Basin (Belgium): International Symposium on Ostracoda, 12th, Prague, Abstracts, p. 21.

Claeys, P., and Casier, J.-G., 1994, Microtektite-like impact glass associated with the Frasnian-Famennian boundary mass extinction: Earth and Planetary Science Letters, v. 122, p. 303–315.

Claeys, P., Casier, J. G., and Margolis, S. V., 1992, Microtektite glass at the Frasnian/Famennian boundary in Belgium: Evidence for an asteroid impact?: Science, v. 257, p. 1102–1104.

Flügel, E., 1982, Microfacies analysis of limestones: Berlin, Springer-Verlag, 633 p.

Geldsetzer, H. H. J., Goodfellow, W. D., McLaren, D. J., and Orchard, M. J., 1987, Sulfur-isotope anomaly associated with the Frasnian-Famennian extinction in Medicine Lake, Alberta, Canada: Geology, v. 15, p. 393–396.

Glass, B. P., 1990, Tektites and microtektites: Key facts and interferences: Tectonophysics, v. 171, p. 393–404.

Govindaraju, K., 1989, Compilation of working values and sample description for 272 geostandards: Geostandards Newsletter, v. 13, special issue, 30 p.

Gromet, P. L., Dymek, R. F., Haskin, L. A., and Korotev, R. L., 1984, The “North American shale composite”: Its compilation of major and trace element characteristics: Geochimica et Cosmochimica Acta, v. 48, p. 2469–2482.

Hut, P., Alvarez, W., Elder, W. P., Hansen, T., Kauffman, E. G., Keller, G., Shoemaker, E. M., and Weissman, P. R., 1987, Comet as a cause of mass extinction: Nature, v. 328, p. 118–126.

Joachimski, M. M., and Buggisch, W., 1993, Anoxic events in the Late Frasnian—Causes of the Frasnian-Famennian faunal crisis?: Geology, v. 21, p. 675–679.

Johnson, J. G., Klapper, G., and Sandberg, C. A., 1985, Devonian eustatic fluctuations in Euramerica: Geological Society of America Bulletin, v. 96, p. 567–587.

Jones, B., and Manning, D., 1994, Comparison of geochemical indices used for the interpretation of paleoredox conditions in ancient mudstones: Chemical Geology, v. 11, p. 111–129.

Jörskog, K. G., Klovan, J. E., and Reyment, R. A., 1976, Geological factor analysis. Methods in geomathematics: Amsterdam, Elsevier, 178 p.

Klinkhammer, G. P., and Palmer, M. R., 1991, Uranium in the oceans: Where it goes and why: Geochimica et Cosmochimica Acta, v. 55, p. 1799–1806.

Kyte, F. T., 1988, The extraterrestrial component in marine sediments: Description and interpretation: Paleoceanography, v. 3, p. 235–247.

Kyte, F. T., Zhou, L., and Wasson, J. T., 1980, Siderophile-enriched sediments from the Cretaceous-Tertiary boundary: Nature, v. 288, p. 651–656.

Kyte, F. T., Zhou, L., and Wasson, J. T., 1988, New evidence on the size and possible effects of a Late Pliocene oceanic asteroid impact: Science, v. 241, p. 63–65.

Kyte, F. T., Leinen, M., Heath, G. R., and Zhou, L., 1992, Cenozoic sedimentation history of the central North Pacific: Inferences from the elemental geochemistry of core LL44-GPC3: Geochimica et Cosmochimica Acta, v. 57, p. 1719–1740.

Lethier, S. F., and Casier, J.-G., 1995, The uppermost Frasnian (Upper Kellwasser) ostracodes from Coumiac (Montagne Noire, France): Revue de Micropaléontologie, v. 38, p. 65–79.

McGhee, G. R., 1989, The Frasnian/Famennian extinction event, *in* Donovan, S. K., ed., Mass extinction: Processes and evidences: London, Belhaven Press, p. 133–151.

McGhee, G. R., Orth, C. J., Gilmore, J. S., and Olsen, E. J., 1984, No geochemical evidence for an asteroidal impact at Late Devonian mass extinction horizon: Nature, v. 308, p. 629–631.

McLaren, D. J., 1982, Frasnian-Famennian extinctions, *in* Silver, L. T., and Schultz, P. H., eds., Geological implications of impacts of large asteroids and comets on the Earth: Geological Society of America Special Paper 190, p. 477–483.

Nicoll, R. S., and Playford, P. E., 1990, Upper Devonian iridium anomaly and the Frasnian-Famennian boundary in the Canning Basin, Western Australia: Geological Society of Australia Abstracts, v. 21, p. 296.

Norusis, M. J., 1991, The SPSS guide to data analysis for SPSS/PC$^+$: Chicago, SPSS Inc., 87 p.

Orth, C. J., Attrep, M., and Quitana, L. R., 1990, Iridium abundance patterns across bioevent horizons in the fossil record, *in* Sharpton, V. L., and Ward, P. D., eds., Global catastrophes in Earth history; an interdisciplinary conference on impact, volcanism and mass mortality: Geological Society of America Special Paper 247, p. 45–59.

Playford, P. E., McLaren, D. J., Orth, C. J., Gilmore, J. S., and Goodfellow, W. D., 1984, Iridium anomaly in the Upper Devonian of the Canning Basin, Western Australia: Science, v. 226, p. 437–439.

Sandberg, C. A., Ziegler, W., Dreesen, R., and Butler, J. L., 1988, Late Frasnian mass extinction: Conodont event stratigraphy global changes and possible causes: Courier Forschungsinstitut Senckenberg, v. 102, p. 267–307.

Schmidt, G. L., Zhou, L., and Wasson, J. T., 1993, Iridium anomaly associated with the Australasian tektite-producing impact: Masses of the impactor and of the Australasian tektites: Geochimica et Cosmochimica Acta, v. 57, p. 4851-4859.

Sepkoski, J. J., Jr., 1982, Mass extinction in the Phanerozoic oceans: A review, *in* Silver, L. T., and Schultz, P. H., eds., Geological implications of impacts of large asteroids and comets on the Earth: Geological Society of America Special Paper 190, p. 283–289.

Sholkovitz, E. R., Landing, W. M., and Lewis, B. L., 1994, Ocean particles chemistry: The fractionation of rare earth elements between suspended particles and seawater: Geochimica et Cosmochimica Acta, v. 58, p. 1567–1579.

Streel, M., and Vanguestaine, M., 1989, Palynomorph distribution in a siliciclastic layer near the Frasnian-Famennian boundary at two shelf facies localities in Belgium: Bulletin Societe Belge Geologie, v. 98, p. 109–114.

Taylor, S. R., and McLennan, S. M., 1985, The continental crust: Its composition and evolution: Oxford, Blackwell, 312 p.

Tyson, R. V., and Pearson, T. H., 1991, Modern and ancient continental shelf anoxia: An overview, *in* Tyson, R. V., and Pearson, T. H., eds. Modern and ancient continental shelf anoxia: Geological Society of London Special Publication 58, p. 1–24.

Turekian, K. K., and Wedepohl, K. H., 1961, Distribution of the elements in some major units of the Earth crust: Geological Society of America Bulletin, v. 72, p. 175–192.

Vine, J. D., and Tourtelot, E. B., 1970, Geochemistry of black shale deposits: A summary report: Economic Geology, v. 65, p. 253–275.

Wang, K., 1992, Glassy microspherules (microtektites) from an Upper Devonian Limestone: Science, v. 256, p. 1546–1549.

Wang, K., Orth, C. J., Attrep, M., Jr., Chatterton, B. D. E., Hou, H., and Geldstzer, H. H. J., 1991, Geochemical evidence for a catastrophic biotic event at the Frasnian/Famennian boundary in south China: Geology, v. 19, p. 776–779.

Wedepohl, K. H., 1969, Composition and abundance of common sedimentary rocks, *in* Wedepohl, K. H., ed., Handbook of geochemistry, Volume 1: Berlin, Springer-Verlag, p. 250–269.

Ziegler, W., and Sandberg, C. A., 1990, The Late Devonian standard conodont zonation: Courier Forschunginstitut Senckenberg, v. 121, 115 p.

Manuscript Accepted by the Society September 14, 1995

Printed in U.S. A.